CHAPTER 6

KINETICS OF CALCIUM MOLYBDATE CRYSTALLIZATION

Contents

6.1 INTRODUCTION

In the preceding chapters (chapters 4 and 5) some attempt has been made to understand the growth characteristics and mechanism, qualitatively, on the basis of observations of different surface features on the as-grown faces. In most systems used for the growth of crystals, nucleation is known to occur heterogeneously, that is at favourable sites within the solution such as the crucible walls or the surface of the solution. Nucleation theory, however, normally describes the process of homogeneous nucleation in which the nuclei are considered to form at random throughout the solution, although estimates of heterogeneous nucleation can also be made. Once a crystal has nucleated in a solution, the growth process involves the transport of solute molecules from the solution to some point on the crystal surface where they become part of the surface. As first suggested by Kossel (1) the growth on a crystal having a flat interface requires some mechanism by which atoms (or the appropriate growth units) will be integrated into the crystal more readily than on the remaining surfaces. This integration may be at the edges of a layer of monatomic thickness which spreads laterally across the crystal surface. Integration

of atoms onto the crystal will occur most readily at vacant sites, or so called "Kinks", along the edges of this layer since an atom entering such a kink will be able to form nearest-neighbour bonds with three atoms in the crystal. The rate of growth of large crystals in solution is normally determined by the rate with which the matter is transferred to the crystals by diffusion or convection (2). When the crystals are relatively small, several phenomena occuring on the surface of the growing crystals may influence the rate of growth. If a crystal which has a stepped interface is in contact with a supersaturated solution, the process of growth may be considered to occur in the following stages :

(a) Transport of solute to the neighbourhood of the crystal surface.

(b) Diffusion through a boundary layer, adjacent to the surface, in which a gradient in the solute concentration exists because of depletion of material at the crystal-solution interface.

(c) Adsorption on the crystal surface.

(d) Diffusion over the surface.

(e) Attachment to a step.

(f) Diffusion along the step.

(g) Integration into the crystal at a kink site.

These elementary phenomena lead to different types of crystallization kinetics.

The mechanism of crystallization of many inorganic materials from high temperature solution has been studied by many workers (3-7). Packter and Roy (8-10) studied some of the crystallization kinetics of alkaline earth metal precipitates, chiefly the alkaline earth metal molybdates (11). It appears that only a preliminary report on the kinetics of crystal growth of calcium molybdate is available in literature. Having grown the crystals (chapter 4) it is in the fitness of the things to study their growth mechanism. It was our aim, therefore, to make detailed and quantitative investigation on the kinetics of crystallization of calcium molybdate with a view to understand the mechanism of growth from the unstirred supersaturated solutions of lithium chloride at 700 and 750°C.

6.2 EXPERIMENTAL DETAILS

6.2.1 Crystallization

The solubility of calcium molybdate in LiCl melt has already been determined in chapter 4. The

observed increase in the solubility with temperature is quite favourable for the crystal growth. From the available solubility data (figure 4.2) appropriate quantities of the flux and the solute were weighed, mixed thoroughly using a pestle and mortar and then packed into a platinum crucible with a loosely fitting lid which suppresses excessive evaporation. The saturated solutions were prepared at a temperature, given by,

$$T_i = T_o + \Delta T$$

where T_o is the temperature at which the crystallization is intended to be studied and $\Delta T = 50^oC$. The charge was heated at T_i for one hour. The charge was deliberately heated at 50^oC above T_o, to ensure removal of any undissolved excess nuclei which might have remained at T_o; failure to carry this out usually resulted in considerable spurious nucleation. The furnace was then rapidly cooled to the crystallization temperature T_o and then soaked for an hour. After soaking, it was cooled at a uniform rate of $5^oC\ hr^{-1}$ for different periods ranging from 1 to 17 hr, after which the crucible was immediately withdrawn from the furnace and the undissolved crystals were separated

from the solidified matrix by leaching with hot distilled water. The crystallization was studied at T_o = 700 and 750°C and the grown crystals were characterized essentially by EDAX and XRD (chapter 5). Crystal sizes were measured by an optical microscope (least count 0.001 cm).

The crystallization was next studied at T_o = 650, 700 and 750°C, but this time the charge was cooled from T_o down to the eutectic (550°C) at 5°C hr^{-1}. The furnace power was then turned off and the crucible allowed to cool down to the room temperature. The effect of variation of crystallization temperature on the final crystal size and the number was also studied.

6.2.2 Measurement of growth parameters

Calcium molybdate crystallized as tetragonal bipyramids with well-developed (011) faces. The average crystal lengths l_t and widths w_t were both measured using a travelling microscope. The l_t (cm) versus t (hr) and w_t (cm) versus t (hr) plots are shown in Figs. 6.1(a) and 6.1(b) respectively. For immediate comparison of the two cases, they have been plotted together also as shown in Fig. 6.2. One clearly observes that the crystal size increases with increasing crystallization

period and, in addition, the growth rate is higher at larger temperatures. However, after about 10 hr of cooling the change in crystal size was appreciably small, giving a final, almost consistent, size l_{fin} and w_{fin}. Probably, the limiting growth rate is imposed by surface kinetic processes, such as desolvation, ledge integration of kinks and steady removal of solvent molecules from the surface. At times, spontaneous nucleation of further crystals might also limit the experimental, maximum feasible, growth rate (3).

6.2.3 Crystallization kinetics

Since l_t is a function of growth time, it is worthwhile to study the degree of crystallization, α_t, which is determined by the ratio of the amount of substance crystallized to the total amount able to crystallize, as defined by Nielsen (12), in the form

$$\alpha_t = \frac{(C_o - C_t)}{(C_o - S)} \qquad (6.1)$$

where C_o is the concentration at $t = 0$, C_t the instantaneous concentration and S ($= C_{sat}$) the solubility. One can also write

$$\alpha_t = l_t^3 / l_{fin}^3 \qquad (6.2)$$

where l_t and l_{fin} are the instantaneous and the final lengths, respectively. It is evident that since l_t is sensitive to the cooling time (Figs. 6.1 and 6.2), α_t becomes a function of the crystallization period and this relationship, plotted for 700 and 750°C, as shown in Fig. 6.3(a), indicates that α_t increases monotonically with time, reaching greater than 0.9 after about 9 hours of crystallization.

Crystal growth rates in unstirred solutions of low permeability are generally controlled by the rate of diffusion of material on different growth faces. The deposition rate of the metal salt ions on growing surfaces from low viscosity LiCl melt, at any time would then be expressed by the relation (12-14).

$$\frac{dl}{dt} = \frac{2\ Sh\ \bar{\phi}_l\ (\epsilon)\ D\ \Delta C_t}{l_t}\ \frac{\rho_f}{\rho_x}\ ,\ \frac{cm}{sec} \qquad (6.3)$$

where Sh is Sherwood dimensionless function, $\bar{\phi}_l\ (\epsilon)$ an overall shape permeability factor, D the diffusion coefficient of metal salt ion Ca^{+2}, ΔC_t the instantaneous

excess $CaMoO_4$ concentration expressed in g/g solution (dl/dt, however, depends on α_t through ΔC_t), ρ_x the crystal density and ρ_f the fluxed-melt density. In the present case of unstirred molten solution where the natural convection is very poor, $Sh \simeq 2$ (14). One therefore obtains

$$\frac{dl}{dt} = \frac{(2 K_{Dl} \Delta C_t)}{l_t} \quad , \quad \text{cm/sec} \qquad (6.4)$$

where K_{Dl} is the rate constant (dependent on the permeability factor) for diffusion-controlled growth of the longer crystal-pyramid side. A general solution of equation (6.4) for all α_t values can be given as

$$I_D(\alpha) = \int_o^{\infty} \frac{d\alpha}{\alpha^{1/3}(1-\alpha)} = \left(\frac{12 K_{Dl} \Delta C_o}{l_{fin}^2} \right) t = \frac{t}{K_D} \qquad (6.5)$$

The rate constant of metal salt deposition, K_D, having the dimension of time, contains all physical constants of the process, including K_{Dl}, ΔC_o and l_{fin}^2. Furthermore, $I_D(\alpha)$ is identified as the dimensionless time, or chronomal, which is a characteristic parameter for diffusion-controlled and polynuclear-layer controlled growth processes. It signifies that if the size of a particle is known at a certain time, one can calculate

back at constant concentration the time at which the particle started with zero size. The integral in (6.5) can be solved using standard methods (15) to give

$$I_D(\alpha) = \frac{1}{2} \ln \left[\frac{(1-\alpha)}{(1-\alpha^{1/3})^3} \right] - \sqrt{3} \tan^{-1} \left[\frac{\sqrt{3}}{1+2\alpha^{-1/3}} \right] \qquad (6.6)$$

This equation really predicts the overall kinetics of crystallization. The values of the diffusion chronomol $I_D(\alpha)$, obtained with the help of Nielsen's table (12) are plotted with time as shown in Fig. 6.3(b) for 700 and 750°C. Again the two curves of Figs. 6.3(a) and 6.3(b) have been plotted together in Fig. 6.4 for ready comparison. The two kind of plots (Fig. 6.4) are seen to be linear up to $\alpha_t \simeq 0.61$ for 700°C and $\alpha_t \simeq 0.65$ for 750°C. Similarly, expressing the rate of diffusion-controlled growth of the shorter side of the crystal bipyramid as

$$\frac{dw}{dt} = \frac{(2 K_{Dw} \Delta C_t)}{w_t} \text{ , cm/sec} \qquad (6.7)$$

The Nielsen's relation for this case would be

$$I_D(\alpha) = \left(\frac{12 K_{Dw} \Delta C_o}{w_{fin}^2} \right) t = t/K_D \qquad (6.8)$$

The graphical plots of α_t and $I_D(\alpha)$ versus t (hr) are shown separately in Figs. 6.5(a) and 6.5(b) respectively and both together, for the purpose of immediate and simultaneous comparison, in Fig. 6.6. Both the plots are seen to be linear up to $\alpha_t \simeq 0.44$ and $\alpha_t \simeq 0.68$ for 700 and 750°C respectively.

It is interesting to find the rate constants K_{D1} and K_{Dw} at different crystallization temperatures from $I_D(\alpha)$ versus t (hr) plots using the relations :

$$K_{D1} = \frac{\text{Grad}\,[I_D(\alpha) \text{ vs } t \text{ (hr) plot}] \times l_{fin}^2}{12\,\Delta C_o} \frac{cm^2}{sec} \qquad (6.9)$$

and

$$K_{Dw} = \frac{\text{Grad}\,[I_D(\alpha) \text{ vs } t \text{ (hr) plot}] \times w_{fin}^2}{12\,\Delta C_o} \frac{cm^2}{sec} \qquad (6.10)$$

The necessary ΔC_o values were estimated from the solubility versus temperature data (chapter 4) and the results are shown in Table 6.1.

Table 6.1 Initial excess solute concentration ΔC_o and rate constant at different temperatures.

Temperature ^oC	ΔC_o (g/g solution)	Rate constant ($cm^2\ sec^{-1}$)	
		$10^{-4}\ K_{Dl}$	$10^{-4}\ K_{Dw}$
700	0.069	0.0776	0.0234
750	0.071	0.01138	0.0526

It is believed that ~~in order~~ for a crystal to grow from solution, the solute must essentially be transported through the solution to the growing surface, desolvated and arranged in conformity with the crystal structure. Therefore, both the diffusion and the convection are important in controlling the growth velocity. But when the crystal is relatively smaller, say 10 μ, convection may be neglected in view of the very low velocity of growth fronts in normal gravity fields. At this stage, when convection is insignificant, crystal growth takes place principally due to Fick's steady diffusional concentration gradients. The fact that this state is established around the crystal at a much faster rate than the rate at which the solution in its close vicinity would be replenished, has been proved by Nielsen (12). This also explains the initially faster growth rate (Fig. 6.2). Such a situation, on an average, exists in the present case up to about 63 % (corresponding to $\alpha_t \simeq 0.61$ at 700 and $\alpha_t \simeq 0.65$ at 750°C) and the remaining growth may, however, be surface reaction controlled, approximated by the relation

$$l_t^3 = l_o^3 + K_R (t - t_o) \qquad (6.11)$$

where K_R is the surface-reaction rate constant.

The fact that the remanant 37 % of growth occurs by surface-reaction needs confirmation. This could not be done experimentally because it is not possible to measure the surface tension of solid substances. though some attempts have been made in this direction (16) with non-convincing results. Nonetheless, the fact that the lateral growth rate is diffusion-controlled to only about 44 % is corroborative of the pyramidal morphology of the grown crystal with its c-axis much larger than either lateral axes.

Further, to understand the effect of crystallization temperature on the final crystal size and the crystal number, the final crystal lengths, l_{fin} and widths, w_{fin} were measured, and the number N of the crystals that grew from 100 g solution was determined from the average crystal lengths, using the relation (17)

$$N = (\Delta W_{tot} / \rho_x f_s l_{fin}^3) \ 100 \text{ g solution}^{-1} \qquad (6.12)$$

where ΔW_{tot} is the total weight of crystals forming

from 100 g solution cooled over the temperature range T_o to T_{eut} (eutectic temperature 550°C), ρ_x is the crystal density and f_s is the shape factor determined by the volume V, given by

$$V = f_s l^3 \qquad (6.13)$$

The effect is shown graphically in Figs. 6.7 and 6.8, revealing that the crystal size increases while the crystal number decreases with the increasing crystallization temperature. This supports the general expectation that the smaller the crystal nuclei concentration the larger will be the crystal size in a growth process.

6.3 CONCLUSIONS

1. The solubility of calcium molybdate in lithium chloride melt increases with increasing temperature; this is fortunately a favourable situation for crystal growth to take place.

2. The degree of crystallization, α_t, increases in the observed period, indicating thereby the crystallization to be homogeneous and uniform throughout.

3. The growth of the longer side of bipyramidal crystals is, in fact, diffusion-rate controlled up to an extent of 61 % and 65 % of crystallization at the studied temperatures of 700 and 750°C, respectively.

4. The crystal size increases while the crystal number decreases with the increasing crystallization temperature.

REFERENCES

1. W. Kossel. (1927)
Nachr. Gesell. Wiss Göttingen, Math-Phys.
K1, 135.

2. A. E. Nielsen. (1969)
Krist. Tech., 4, 17.

3. R. A. Laudise. (1963)
"The Art and Science of Growing Crystals"
(ed.) J. J. Gilman (New York : John Wiley)
p. 252.

4. F. A. Kroger. (1964)
"Chemistry of Imperfect Crystals"
(Amsterdam : North-Holland) P. 31.

5. E. A. D. White. (1964)
Tech. Inorg. Chem., 4, 31.

6. J. B. Schroedger and R. C. Linares. (1966)
Prog. Ceram. Sci., 4, 195.

7. D. Elwell and H. J. Scheel. (1975)
"Crystal Growth from High-Temperature
Solutions", (Academic Press, London).

8. A. Packter and B. N. Roy. (1973)
J. Crystal Growth, 18, 86.

9. A. Packter and B. N. Roy. (1974)
Kristall und Technik, 9, 1351.

10. A. Packter and B. N. Roy. (1975)
Kristall und Technik, 10, 385.

11. A. Packter. (1977)
Kristall und Technik, 12, 729.

12. A. E. Nielsen. (1964)
"Kinetics of Precipitation"
(Pergamon Press, Oxford) Chapter 3.

13. J. W. Mullin. (1961)
"Crystallization" (London : Butterworths)
Chapter 3.

14. R. E. Treybal. (1968)
"Mass Transfer Operation"
(New York, McGraw Hill) Chapter 3.

15. V. K. Lamer and R. H. Dinegar. (1950)
J. Am. Chem. Soc., 72, 4847.

16. V. D. Kuznetsov. (1957)
"Surface Energy of Solids" (London : HMSO)
translated from Russian.

17. B. N. Roy and A. Packter. (1980)
J. Crystal Growth, 49, 368.

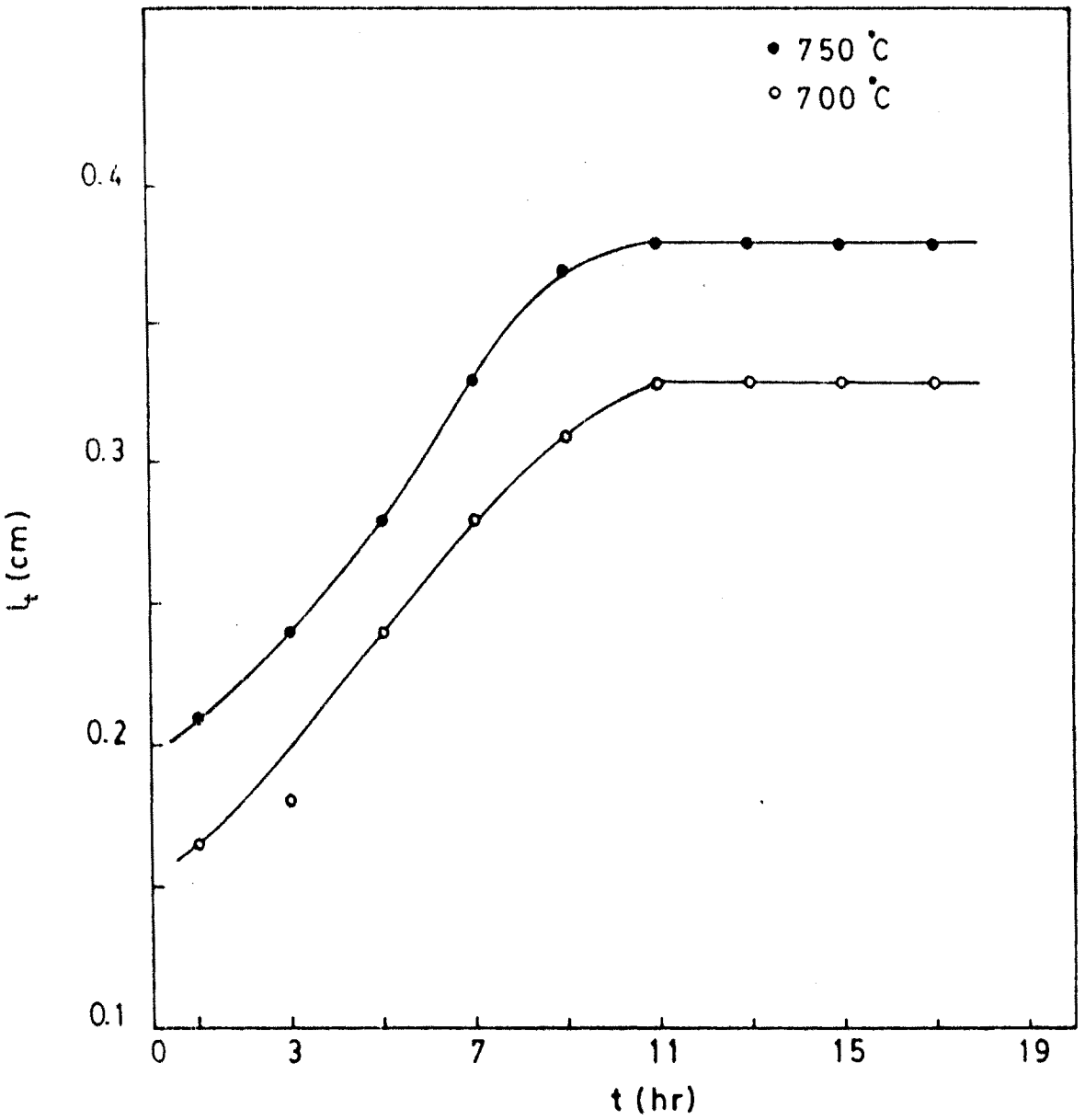

Fig. 6.1(a) The variation of average crystal length versus cooling periods, for 700 and 750°C.

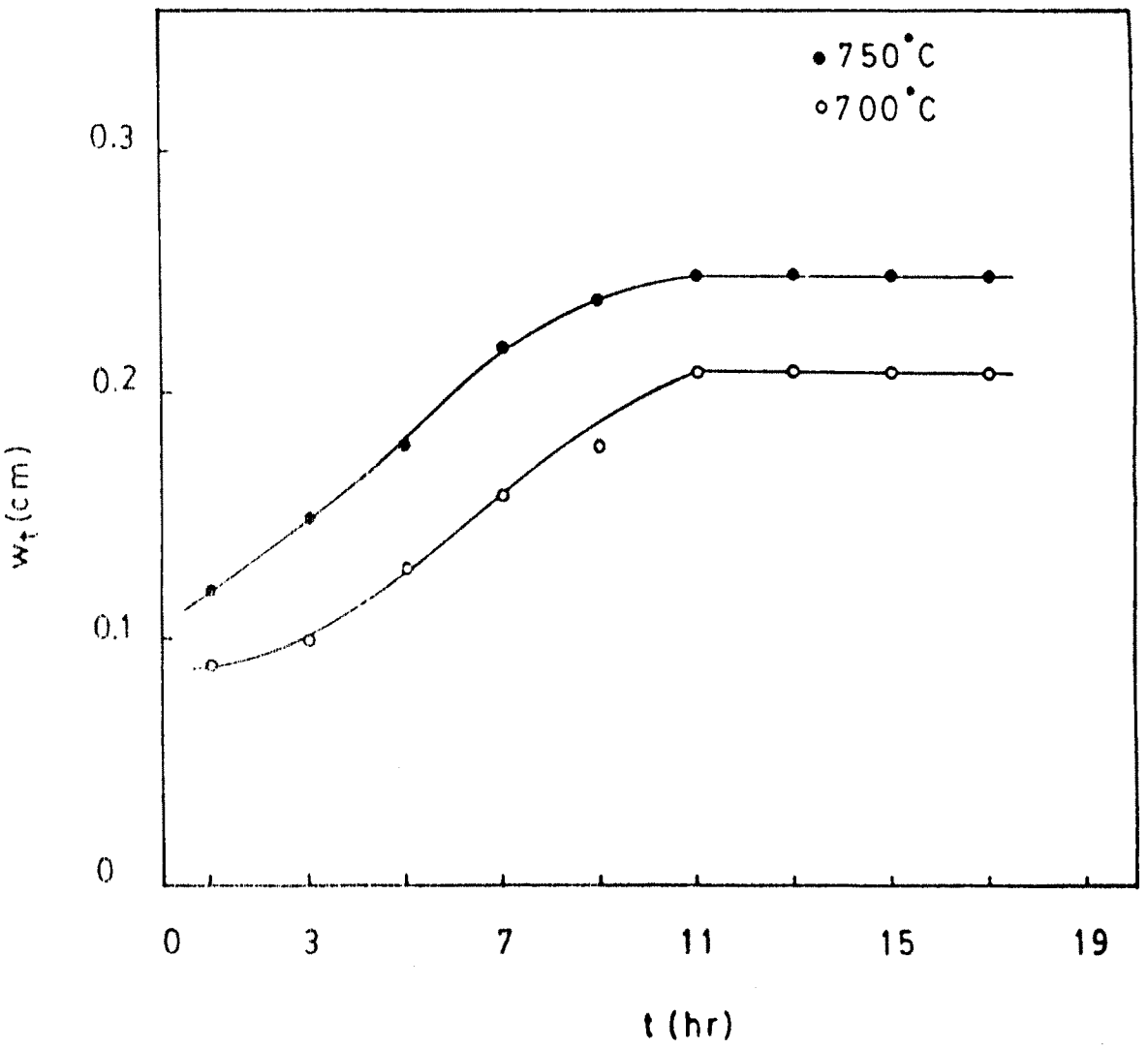

Fig.6.1(b) The variation of average crystal width versus cooling periods, for 700 and 750 °C.

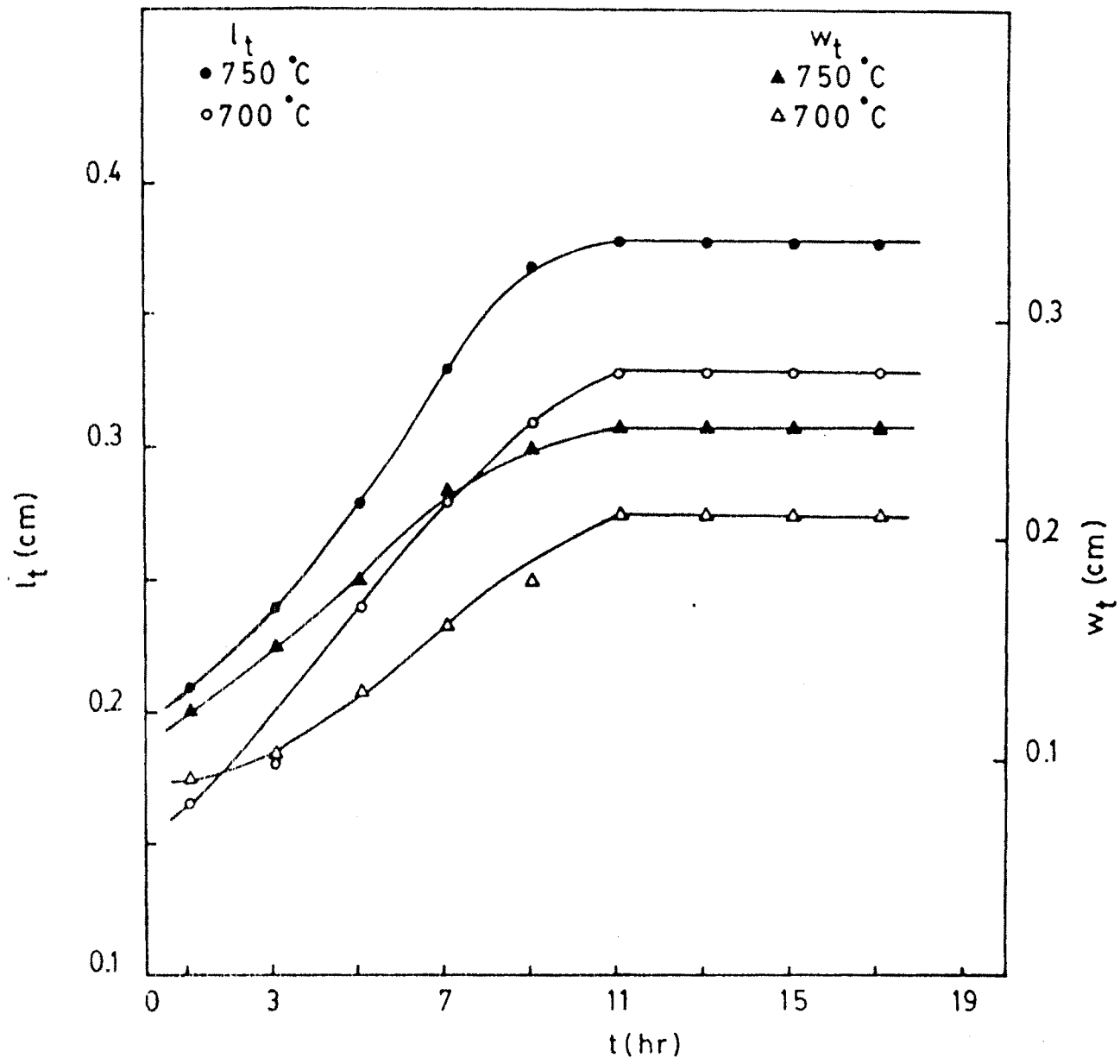

Fig. 6.2 The variation of average crystal length and width versus cooling periods for 700 and 750°C.

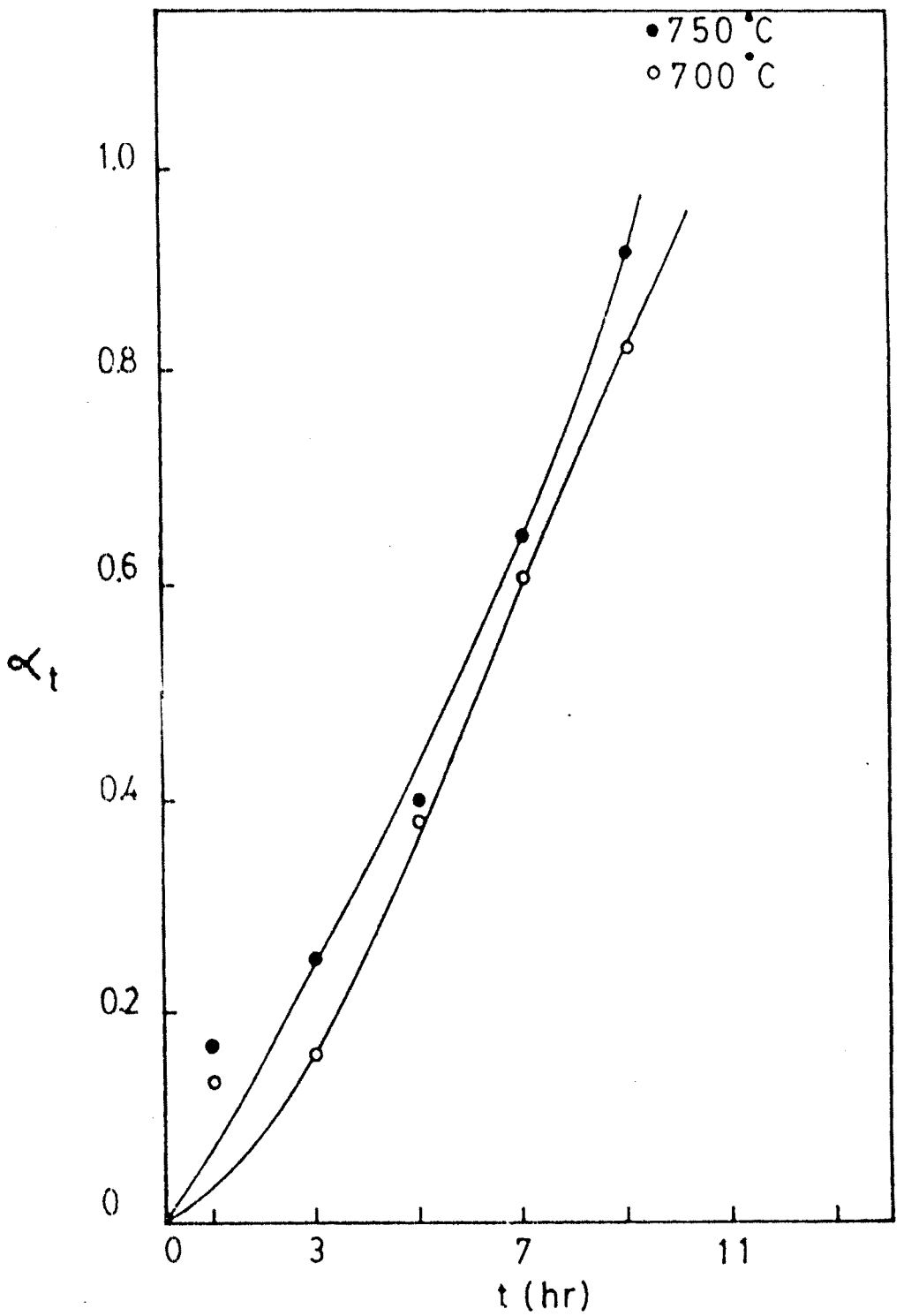

Fig. 6.3(a) The degree of crystallization, α_t, versus cooling periods, for 700 and 750°C, for length.

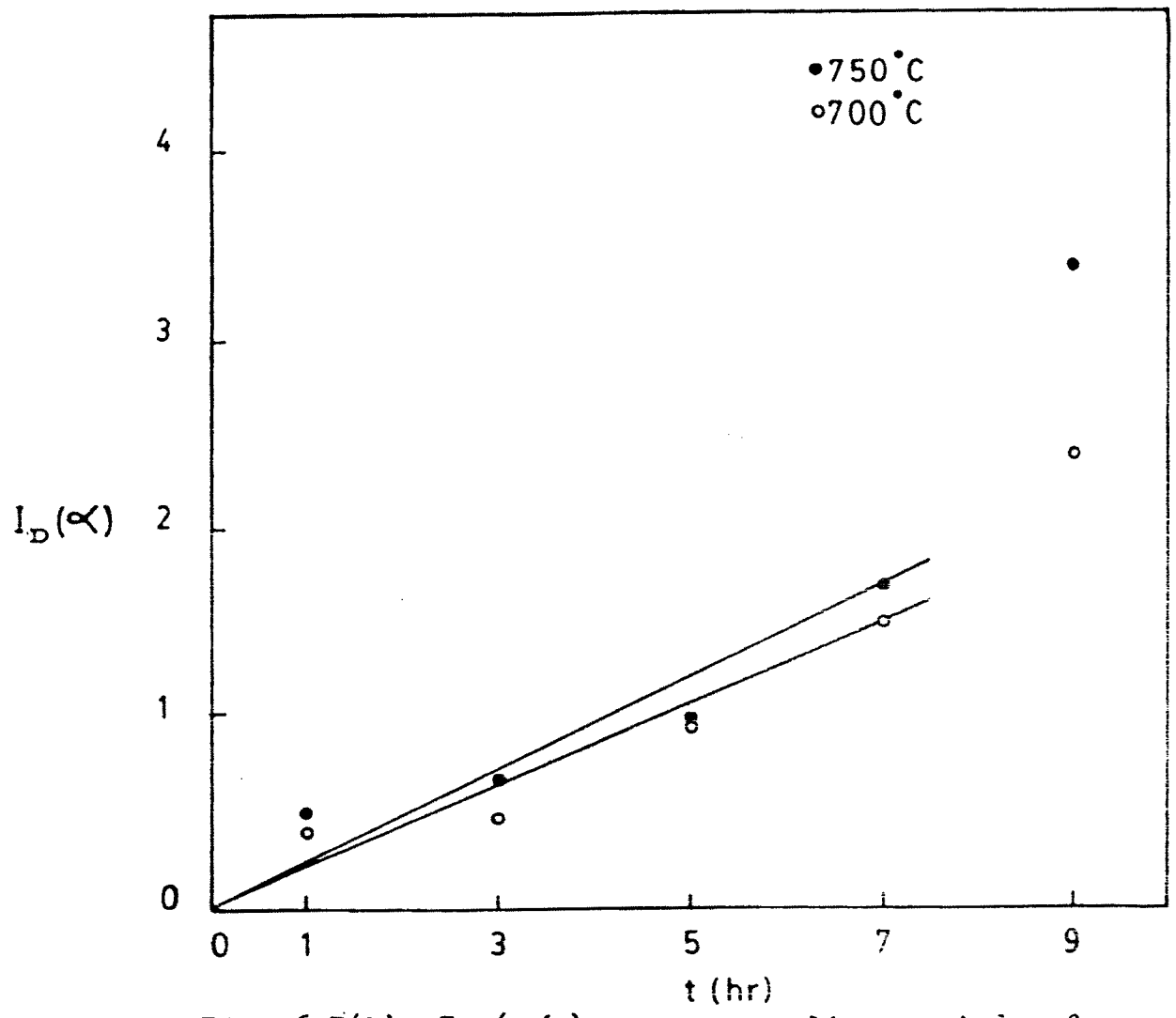

Fig. 6.3(b) I_D ($\propto$) versus cooling periods, for 700 and 750°C, for length.

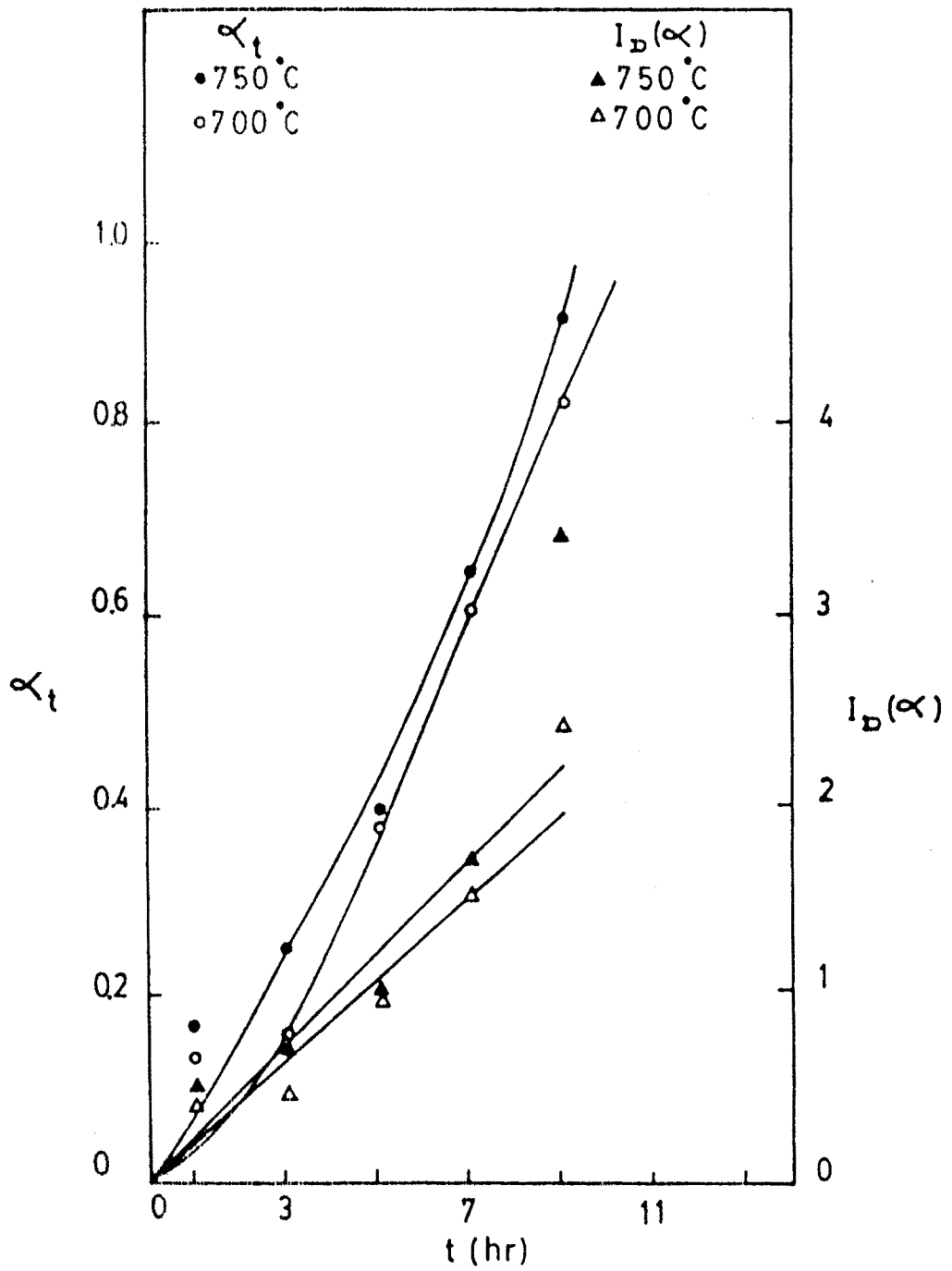

Fig. 6.4 The degree of crystallization, α_t, and I_D (α) versus cooling periods, for 700 and 750°C, for length.

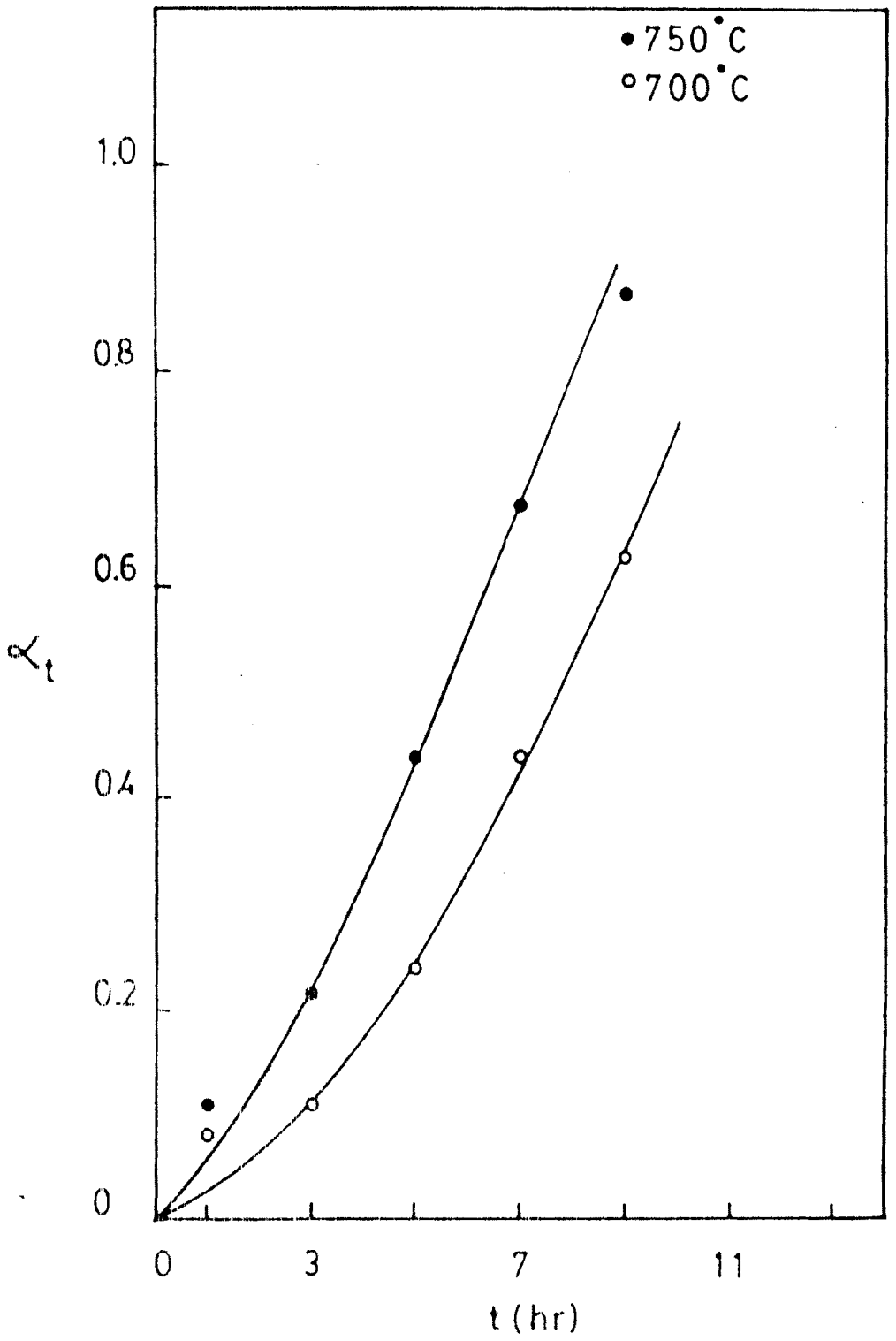

Fig. 6.5(a) The degree of crystallization, α_t, versus cooling periods for 700 and 750°C, for width.

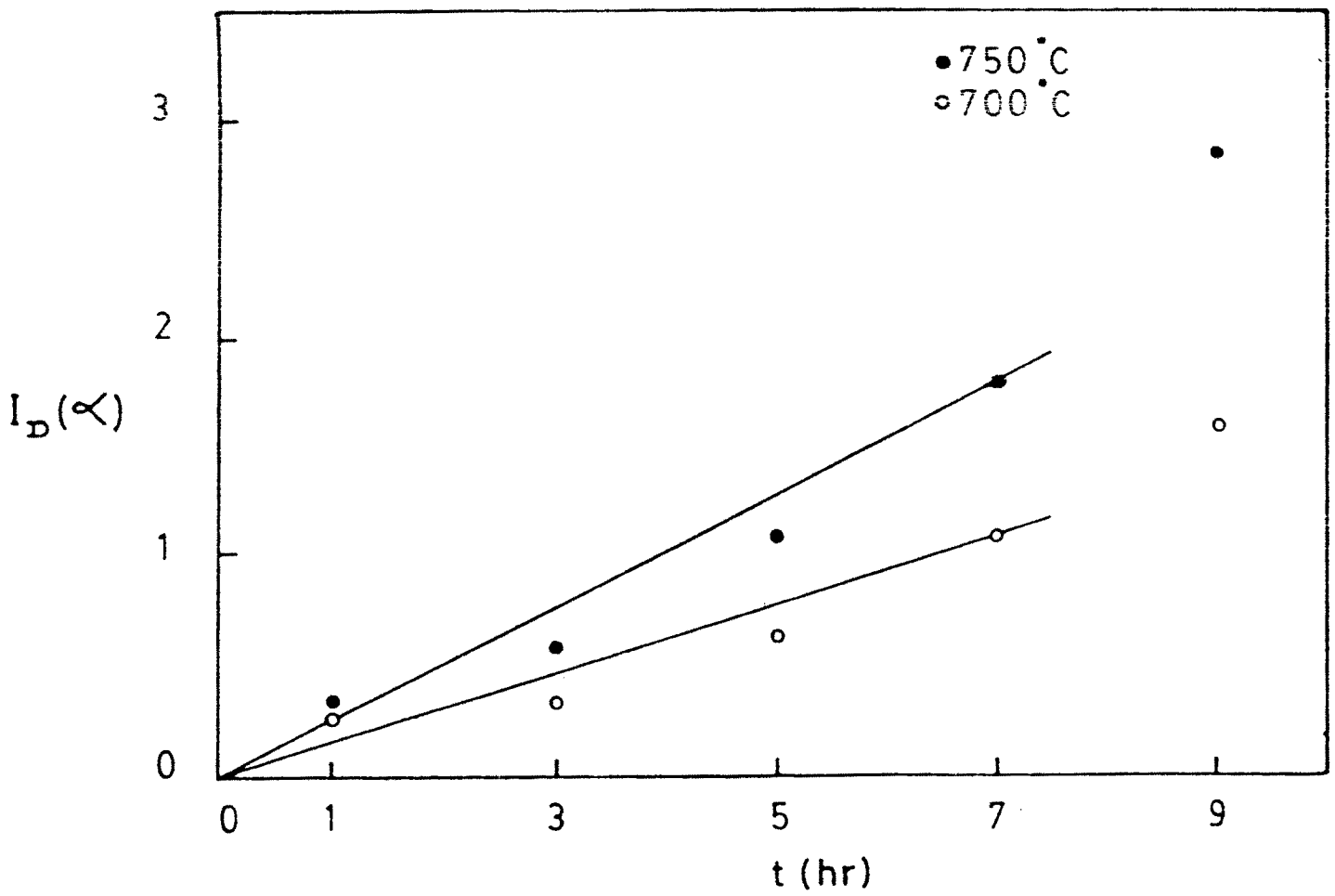

Fig. 6.5(b) I_D (α) versus cooling periods, for 700 and 750°C, for width.

(127)

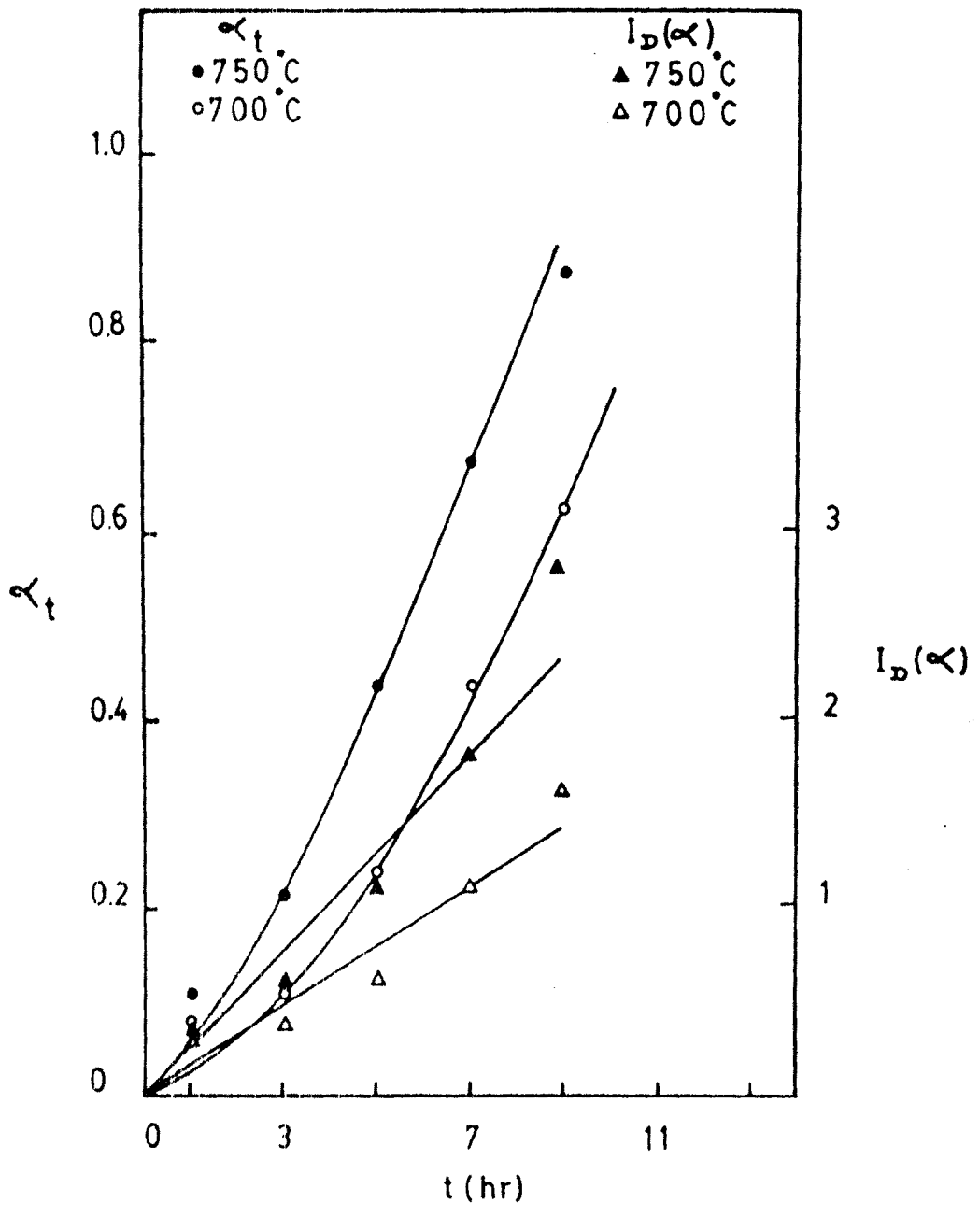

Fig. 6.6 The degree of crystallization, α_t, and $I_D(\alpha)$ versus cooling periods, for 700 and 750°C, for width.

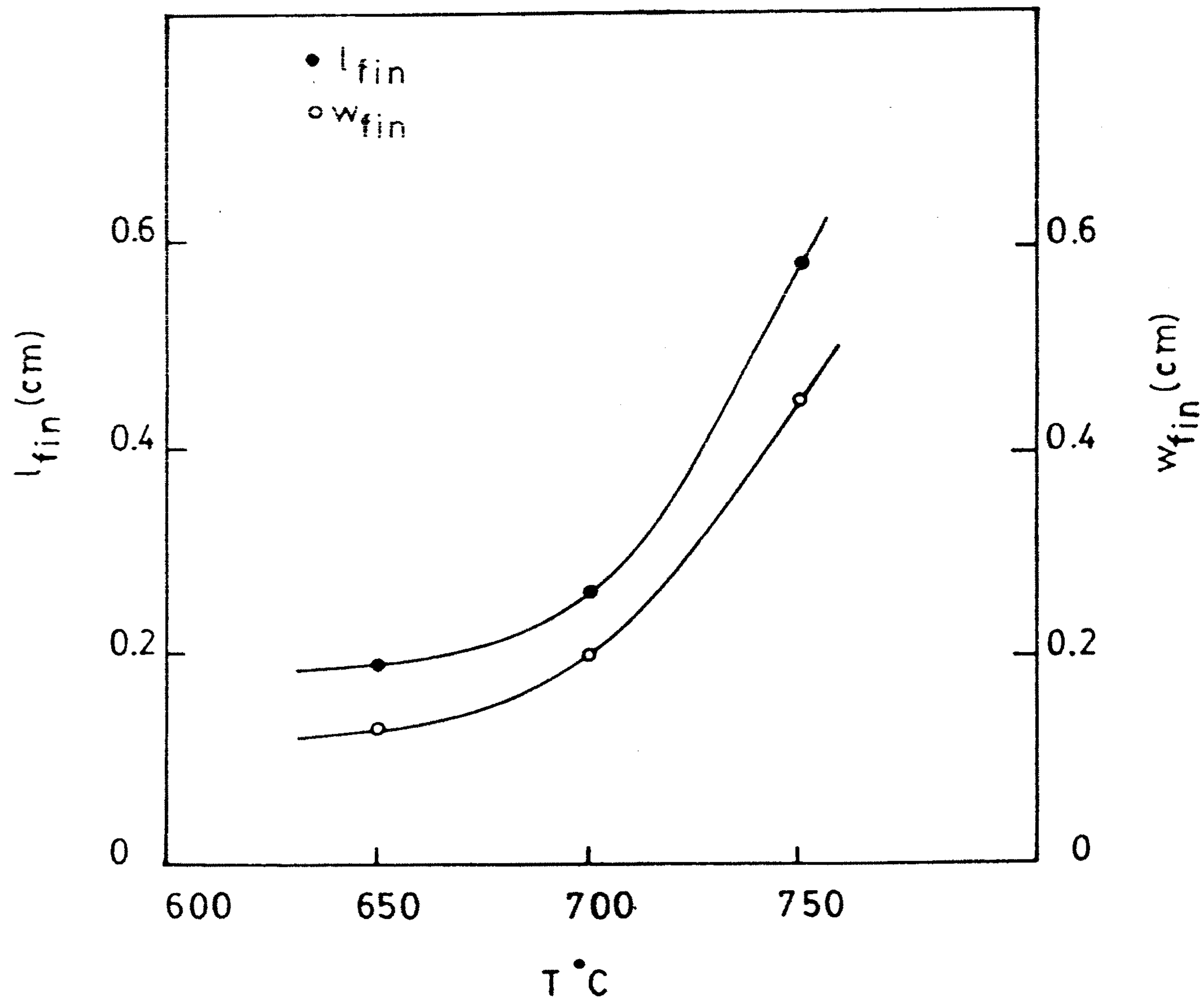

Fig. 6.7 The variation of final crystal length and width against crystallization temperature.

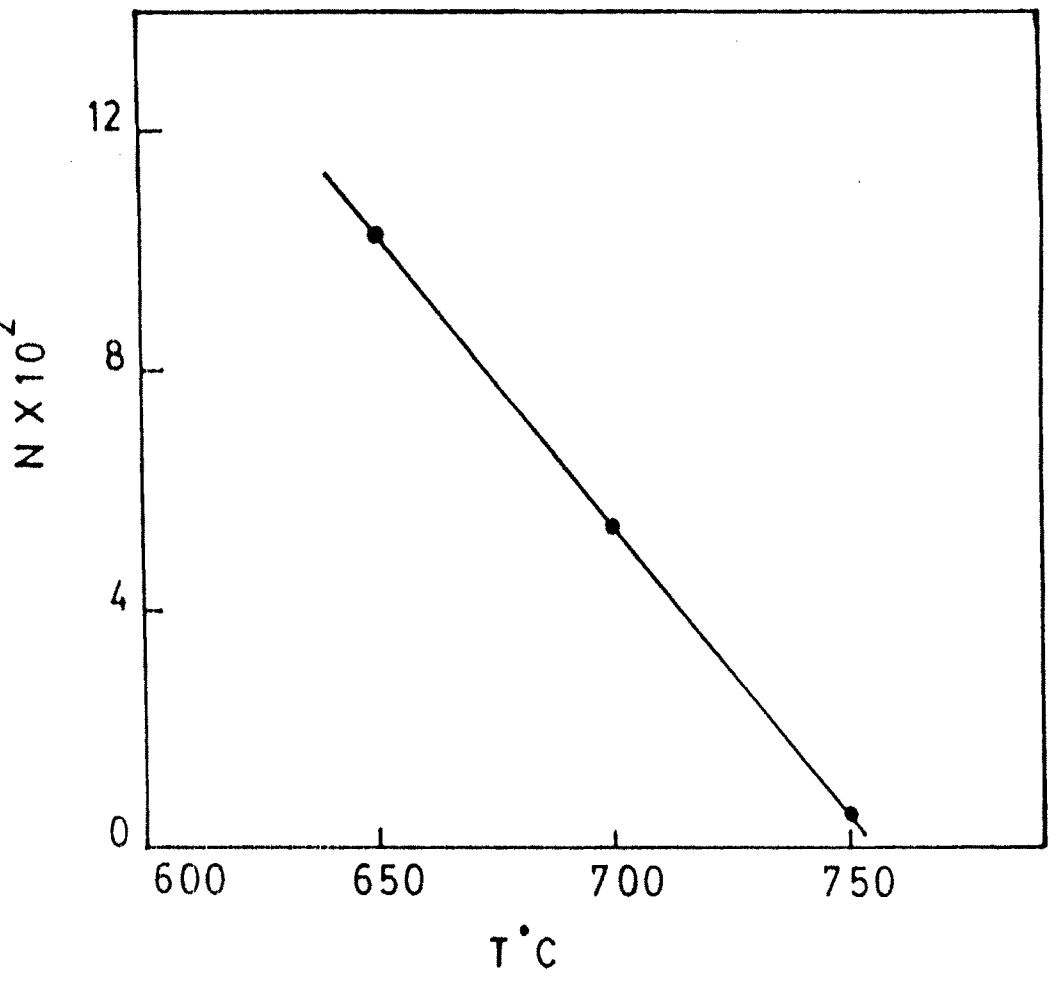

Fig. 6.8 The variation of crystal number against crystallization temperature.